

Direct measurements of constrained Brownian motion of an isolated sphere between two walls

Binhua Lin,* Jonathan Yu, and Stuart A. Rice

The James Franck Institute, The University of Chicago, Chicago, Illinois 60637

(Received 22 November 1999; revised manuscript received 2 June 2000)

We report the results of direct measurements, using video microscopy in combination with optical tweezers, of constrained diffusion of an isolated uncharged PMMA sphere in a density-matched fluid confined between two parallel flat walls. Our experimental methodology allows us to study the hindered diffusion of the sphere as an explicit function of its distance from the walls, without interference from sedimentation or from electrostatic interaction between the particle and the walls. The measured diffusion coefficients are used to test the predictions of the wall drag effect predicted by several approximate theoretical analyses. We find a quantitative agreement with the behavior predicted using a hydrodynamic analysis that independently superimposes the wall drag effects arising from each wall. Our results imply, indirectly, that neglect of multiple interactions with the colloid sphere of the perturbations of the pressure and velocity fields induced by each wall leads to an underestimate of the influence of the wall on the drag force experienced by the particle.

PACS number(s): 82.70.Dd, 83.70.Hq, 66.10.Cb, 65.40.+g

I. INTRODUCTION

When a colloidal sphere suspended in a quiescent fluid is close to a flat wall, the Stokes drag force acting on it is increased relative to that when far from the wall and, therefore, its diffusion coefficient is smaller than that when far from the wall. The increase of the drag force is attributed to the alteration of the hydrodynamic interaction between the colloid particle and the fluid generated by the boundary condition imposed by the nearby wall. The motion of the sphere also becomes anisotropic because the drag force parallel to the wall is less than that perpendicular to the wall. Similar effects occur when a colloidal sphere is confined in a small gap between two flat walls.

Although a simple phenomenon, constrained diffusion of an isolated microscopic sphere between two walls provides us with a model system with which to understand the behavior of more complex systems whose boundaries can be modeled as effective walls. Some examples of those more complex systems are fine particles migrating in porous media, macromolecules diffusing in membranes [1], and cells interacting with surfaces [2]. Constrained diffusion also influences the settling of colloidal particles near fluid-solid boundaries, and other processes that depend on the balance between inter-particle and hydrodynamic forces [3]. Clearly, a detailed understanding of the wall-drag effect that acts on an isolated sphere is necessary to distinguish between hydrodynamic effects due to sphere-wall interaction and those due to sphere-sphere interaction.

The basic theoretical analysis of the influence of a flat wall (or walls) on the hydrodynamic drag force acting on a nearby isolated object was developed many years ago. It is based on the solution to the linear hydrodynamic equations obtained under the creeping motion approximation (the Stokes equations), and is applicable in the regime of low Reynolds number hydrodynamics. Because of the linearity of

the Stokes equations, the drag force on the sphere can be separated into independent components parallel and perpendicular to the wall [4]. Although there are some exact solutions to these equations [1,5–8], these are applicable only to special particle-wall configurations; they are also complicated and difficult to apply. For this reason most investigators have analyzed experimental data using approximate solutions for the modified drag force, based on the so-called “method of reflections” [4,9]. One of the goals of this paper is to provide a detailed test of the predictions made by these approximate solutions of the dependence of the diffusion coefficient on the wall-particle separation.

We have been able to measure the diffusion coefficients of a PMMA sphere parallel to and perpendicular to the walls as a function of both the distance of the sphere from the walls and the separation of the walls. The results of these experiments provide a detailed test of the behavior predicted using hydrodynamic analyses of the perturbation of the flow around a sphere by a nearby wall. Specifically, we find that a hydrodynamic analysis that assumes an independent superposition of the extra drag effects associated with each wall provides an accurate representation of the experimental data. Our results imply, indirectly, that neglect of multiple interactions with the colloid sphere of the perturbations of the pressure and velocity fields induced by each wall leads to an underestimate of the influence of the wall on the drag force experienced by the particle.

Several reports of tests of the available theoretical predictions for the influence of hydrodynamic interference on the behavior of a particle near a boundary have been published. Consider, first, the case of macroscopic particles. For example, an increase in the drag force on a macroscopic sphere moving near a wall implies that the settling rate of a sphere is decreased. This wall effect was investigated directly by using a multiple image technique to film the sedimentation of a nylon sphere (a few millimeters in diameter), approaching a bottom plane in a quiescent fluid [5,10–12]. The drag force on the sphere that is deduced from its sedimentation rate agrees very well with that given by Brenner’s exact solution for this geometry [see Eq. (6)] [5].

*Corresponding author. Email address: binhua@cars.uchicago.edu

Consider, now, the case of microscopic particles subject to Brownian motion. The particle diffusion coefficient, represented in the Stokes-Einstein form, can be used to monitor the hydrodynamic wall effects if suitable experiments can be carried out. Colloidal suspensions are ideal for such experiments, because the particles are small enough to be subject to Brownian motion, yet large enough that the motion of the host fluid can be described in the hydrodynamic limit. Several experimental studies of the constrained diffusion of colloidal spheres near a flat plate or between two flat plates have been reported, all of which used charged colloids. In most of these experiments photon correlation spectroscopy was used to obtain the ensemble averaged diffusion coefficient in a dilute solution, by extrapolation of the concentration dependence of measurements of the intensity autocorrelation function [9,13–16]. In some of the experiments the diffusive motion of an isolated colloidal sphere was studied by imaging and analyzing its motion using total internal reflection microscopy [17,18], digital video microscopy [19], reflection interference contrast microscopy [20], photonic force microscopy [2], and atomic force and optical force microscopy [21]. All of these experiments have shown that the diffusion of a particle, or particles, near a wall is hindered, and all of the observations are qualitatively consistent with the theoretical predictions. However, none of the experiments reported to date provide a *detailed direct* test of the variation of the particle diffusion coefficient with distance from the walls.

In this paper we report the results of an experimental study, using digital video microscopy, of constrained Brownian motion of an isolated uncharged PMMA sphere ($\approx 1 \mu\text{m}$ diameter) confined between two parallel flat walls. The PMMA spheres were suspended in a density-matched fluid to eliminate sedimentation. The position of a sphere with respect to the walls and its diffusion range were controlled with optical tweezers. The separation of the walls was measured *in situ* by the use of reference spheres fixed on the walls.

Our experimental method avoids the following difficulties in the previous experiments. First, in the experiments reported to date, neither the distance of the colloidal sphere from the boundary nor its extent of motion were controlled. Consequently, the diffusion coefficient was not measured as an explicit function of the sphere-wall separation. What has been measured, instead, is an average of the diffusion coefficient along the direction perpendicular to the walls, weighted using a model distribution function for the positions of the colloid particles under the influence of both the walls and gravity [9,14,19]. Moreover, in the analyses of the data reported to date, despite the use of charged colloid spheres, the effect of electrostatic interaction between the charged spheres and the walls was neglected. This neglect compromises the interpretation of the data, because the charged colloid-wall interaction depends on the effectiveness of ionic screening, the existence of charges on the walls, the mobility of those wall charges, etc. [22–24]. Clearly, the measurements reported test the integrated effect of the wall proximity on the particle diffusion coefficient, but not the distance dependence of that effect.

Second, in all of the reported experiments the size of the confining cavity was assumed to be the same as that of the spacers used to make the cavity. Large errors may be introduced by this assumption because it is very difficult to fab-

ricate cavities that are a few microns in spacing, and uniform over a distance of several millimeters. Errors in the cell thickness, hence also the particle distance from a wall, are masked by the integration over particle position used to interpret the measurements.

II. WALL-DRAG EFFECTS ON AN ISOLATED CONFINED BROWNIAN SPHERE

A hard sphere with radius a , moving with velocity \mathbf{U} in an unbounded quiescent fluid of viscosity η , experiences a hydrodynamic drag force opposite to its direction of motion. If there is no slip at the boundary between the hard sphere and the fluid, in the low Reynolds number limit this drag force is (Stokes Law)

$$\mathbf{F}_0 = -6\pi\eta a\mathbf{U}. \quad (1)$$

The diffusion coefficient D_0 of the sphere is then given by the Stokes-Einstein relation

$$D_0 = \frac{k_B T}{6\pi\eta a}, \quad (2)$$

with k_B the Boltzmann constant and T the temperature of the system.

When the sphere is close to a flat wall or is confined between two flat walls, the drag force increases and its diffusion is hindered. Because of the linearity of the Stokes equations, the drag force can be separated into independent components for motion parallel and perpendicular to the wall. The expressions for the parallel and perpendicular components of the wall-drag force are conventionally represented

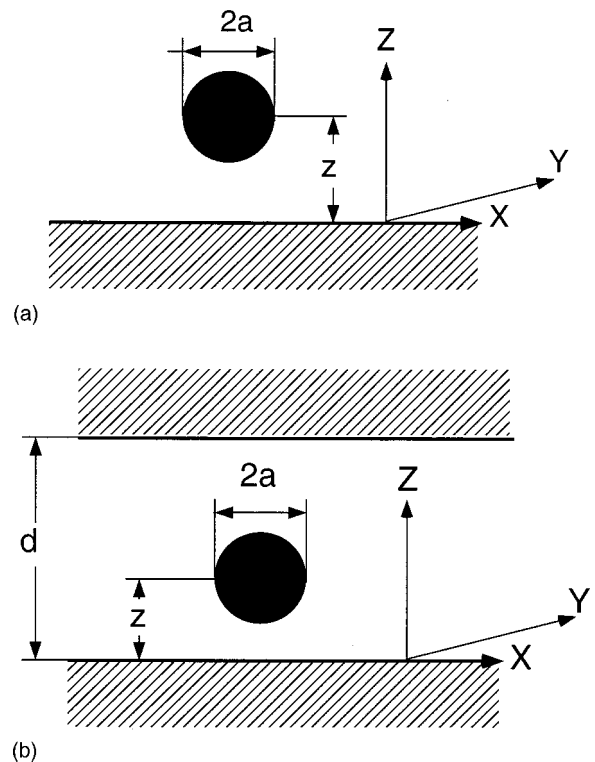


FIG. 1. Schematic representation of a Brownian particle close to one flat wall (a) or confined between two flat walls (b).

in the form of correction factors λ_{\parallel} and λ_{\perp} , multiplying the drag force in an unbounded liquid. These expressions are

$$\mathbf{F}_{\parallel} = -6\pi\eta a \mathbf{U}\lambda_{\parallel} = \mathbf{F}_0\lambda_{\parallel} \quad (3)$$

and

$$\mathbf{F}_{\perp} = -6\pi\eta a \mathbf{U}\lambda_{\perp} = \mathbf{F}_0\lambda_{\perp}. \quad (4)$$

Consequently, the diffusion coefficients for parallel and perpendicular motion of the sphere relative to the wall are

$$\lambda_{\perp}^{-1} = \frac{D_{\perp}}{D_0} = \left\{ \frac{4}{3} \sinh \alpha \sum_{n=1}^{\infty} \frac{n(n+1)}{(2n-1)(2n+3)} \left[\frac{2 \sinh(n+1)\alpha + (2n+1)\sinh \alpha}{4 \sinh^2(n+1/2)\alpha - (2n+1)^2 \sinh^2 2\alpha} - 1 \right] \right\}^{-1}, \quad (6)$$

where $\alpha = \cosh^{-1}(z/a)$ (z is the distance from the center of the sphere with radius a to the wall).

The most commonly used representations of λ_{\parallel} and λ_{\perp} are approximate. These representations are derived using the so-called ‘‘method of reflections.’’ The motion of a sphere near a wall induces a pressure and velocity distribution in the adjacent fluid. The method of reflections is an iterative series solution technique that decomposes the velocity and the pressure fields into a linear superposition of terms of successively higher order in the number of wall and sphere boundary interactions. The terms in the expansion are constrained to alternately satisfy the boundary conditions on the sphere and on the confining walls (see Refs. [4,9] for details). The solutions for λ_{\parallel} and λ_{\perp} obtained with this method are usually expressed as a power series in (a/z) . For λ_{\perp} one finds, for a sphere moving near one flat wall, inclusive of terms to order $(a/z)^3$ [4],

$$\lambda_{\perp}^{-1} = \frac{D_{\perp}}{D_0} \cong 1 - \frac{9}{8} \left(\frac{a}{z} \right) + \frac{1}{2} \left(\frac{a}{z} \right)^3 + O \left(\frac{a}{z} \right)^4. \quad (7)$$

Using the same method, for λ_{\parallel} one finds, for a sphere moving near one flat wall, inclusive of terms to order $(a/z)^5$ [4],

$$\lambda_{\parallel}^{-1} = \frac{D_{\parallel}}{D_0} \cong 1 - \frac{9}{16} \left(\frac{a}{z} \right) + \frac{1}{8} \left(\frac{a}{z} \right)^3 - \frac{45}{256} \left(\frac{a}{z} \right)^4 - \frac{1}{16} \left(\frac{a}{z} \right)^5 + O \left(\frac{a}{z} \right)^6. \quad (8)$$

Frequently, only the first order approximations [4,25]

$$\lambda_{\parallel}^{-1} = \frac{D_{\parallel}}{D_0} \cong 1 - \frac{9}{16} \left(\frac{a}{z} \right) + O \left(\frac{a}{z} \right)^3 \quad (9)$$

and [4,9]

$$\lambda_{\perp}^{-1} = \frac{D_{\perp}}{D_0} \cong 1 - \frac{9}{8} \frac{a}{z} + O \left(\frac{a}{z} \right)^3 \quad (10)$$

$$D_{\parallel} = \frac{k_B T}{6\pi\eta\lambda_{\parallel}a} = \lambda_{\parallel}^{-1} D_0,$$

$$D_{\perp} = \frac{k_B T}{6\pi\eta\lambda_{\perp}a} = \lambda_{\perp}^{-1} D_0. \quad (5)$$

However, even in the low Reynolds number limit, the exact solutions for the effective wall drag force typically do not have a closed analytical form, and they are difficult to apply [1,6–8]. One exception is the exact solution for λ_{\perp} derived by Brenner [5] for a sphere moving near one flat wall [illustrated in Fig. 1(a)], namely,

are used to analyze experimental data.

Figure 2 displays the predicted values of D_{\parallel}/D_0 and D_{\perp}/D_0 as functions of z/a for an isolated sphere near one flat wall. The differences between the respective exact and approximate values of D_{\parallel}/D_0 and D_{\perp}/D_0 are insignificant ($<1\%$) when $(z/a) > 1.5$. The inset in Fig. 2, plotted in a log-log representation, magnifies the differences between the correction factors calculated from Eq. (6) and Eqs. (8)–(10). The first order approximations, with their appealing simple forms, are sufficiently accurate except when the sphere is very close to the wall.

The method of reflections fails to yield an analytical solution for the drag force acting on a sphere located at an arbitrary point between two parallel flat walls [as illustrated in Fig. 1(b)] except for very limited special cases [4]. For example, if the sphere is located exactly in the midplane

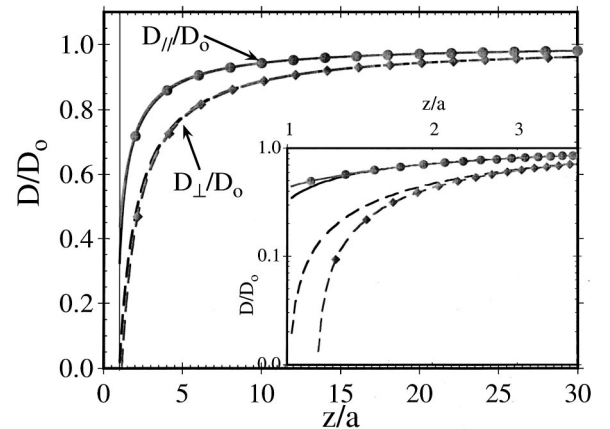


FIG. 2. Predicted values of D_{\parallel} and D_{\perp} for an isolated sphere near one flat wall, normalized by D_0 . The solid and dashed lines are the more accurate values of D_{\parallel}/D_0 and D_{\perp}/D_0 calculated from Eqs. (8) and (6), respectively. The solid and dashed lines with symbols are the values of D_{\parallel}/D_0 and D_{\perp}/D_0 calculated from the first order approximations given in Eqs. (9) and (10), respectively. The inset with log-log scales magnifies the difference between the first order approximation and the more accurate results for D_{\parallel}/D_0 and D_{\perp}/D_0 when $z/a \sim 1$.

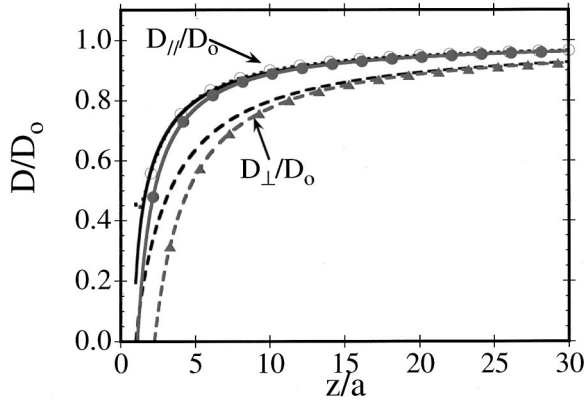


FIG. 3. Predicted values, using the LSA (see text), of D_{\parallel}/D_0 and D_{\perp}/D_0 for an isolated sphere in the midplane ($z \equiv d/2$) between two parallel flat walls. The solid and dashed lines are D_{\parallel}/D_0 and D_{\perp}/D_0 , respectively, calculated using Eqs. (6) and (8) as single wall correction factors. The solid and dashed lines with symbols are the results obtained using the first order approximations [Eqs. (9) and (10)] as single wall correction factors. For comparison, the D_{\parallel}/D_0 calculated from the method of reflections [Eq. (11)] is plotted as a dotted line.

between two flat walls separated a distance d ($z = d/2$), Faxen [4] showed that the correction factor for the drag force due to two walls, $\lambda_{\parallel}^{\text{II}}$, is given as

$$(\lambda_{\parallel}^{\text{II}})^{-1} = \frac{D_{\parallel}}{D_0} \cong 1 - 1.004 \left(\frac{a}{z}\right) + 0.418 \left(\frac{a}{z}\right)^3 + 0.21 \left(\frac{a}{z}\right)^4 - 0.169 \left(\frac{a}{z}\right)^5 + O\left(\frac{a}{z}\right)^6. \quad (11)$$

Several approximate analyses of the hydrodynamic drag on a sphere situated between two walls have been based on the use of a linear superposition of single-wall effects. The simplest of these analyses assumes it is adequate to *independently* superimpose the effects of the drag force on the sphere from each wall [4,14]. In this case the drag force on the sphere, F^{II} (either parallel or perpendicular to the wall), is taken to be the sum of the force on the sphere in an unbounded fluid, F_0 , plus the correction terms, at the position of the sphere, for each wall as if the other were absent. That is,

$$f^{\text{II}} = F_0 \lambda^{\text{II}} \cong F_0 + F_0(\lambda_{\text{wall1}}^{\text{I}} - 1) + F_0(\lambda_{\text{wall2}}^{\text{I}} - 1) = F_0(\lambda_{\text{wall1}}^{\text{I}} + \lambda_{\text{wall2}}^{\text{I}} - 1). \quad (12)$$

In Eq. (12), λ^{II} is the two-wall correction factor, and $\lambda_{\text{wall1}}^{\text{I}}$ and $\lambda_{\text{wall2}}^{\text{I}}$ are the single wall correction factors. This formulation of the drag force is referred to as the linear superposition approximation (LSA) in this paper. The form taken by λ^{II} is

$$\lambda^{\text{II}} \cong \lambda_{\text{wall1}}^{\text{I}} + \lambda_{\text{wall2}}^{\text{I}} - 1 = \lambda^{\text{I}}(z) + \lambda^{\text{I}}(d-z) - 1. \quad (13)$$

Figure 3 displays D_{\parallel}/D_0 and D_{\perp}/D_0 as functions of z/a , calculated using Eqs. (8) and (6) for $\lambda_{\parallel}^{\text{I}}$ and $\lambda_{\perp}^{\text{I}}$, respectively, for the special case in which the sphere is in the midplane between the two plates ($z = d/2$). In this figure we also show

D_{\parallel}/D_0 as a function of z/a , calculated using Eq. (11). The deviation between the approximate values [using Eq. (13)] and exact values [using Eq. (11)] of D_{\parallel}/D_0 is less than 1% when $z/a \geq 1.7$. This comparison provides a test of the linear superposition approximation.

When the sphere is not very close to the walls, simpler expressions for the two-wall hydrodynamic correction factors can be obtained from the combination of Eq. (13) and Eqs. (9) and (10). It is found that [4]

$$(\lambda_{\parallel}^{\text{II}})^{-1} = \frac{D_{\parallel}}{D_0} \cong 1 - \frac{9}{16} \left[\left(\frac{a}{z}\right) + \left(\frac{a}{d-z}\right) \right] + O\left(\frac{1}{z/a}\right)^2 \quad (14)$$

and

$$(\lambda_{\perp}^{\text{II}})^{-1} = \frac{D_{\perp}}{D_0} \cong 1 - \frac{9}{8} \left[\left(\frac{a}{z}\right) + \left(\frac{a}{d-z}\right) \right] + O\left(\frac{1}{z/a}\right)^2. \quad (15)$$

Calculated values of D_{\parallel}/D_0 and D_{\perp}/D_0 using Eqs. (14) and (15) are also plotted in Fig. 3. When the plate separation is only slightly greater than the sphere diameter, the first order approximations overestimate the wall effects much more than the higher order approximations do. Note, however, that when $z/a > 4$, the error in $\lambda_{\parallel}^{\text{II}}$ is less than 5%.

A seemingly superior approximation for the hydrodynamic drag induced on a particle by the presence of two nearby flat walls is based on the coherent superposition of the influences of the single walls [4,9]. The two-wall correction factor is, in this approximation,

$$\lambda^{\text{II}}(z) \cong 1 + \sum_{n=0}^{\infty} [\lambda^{\text{I}}(z+nd) - 1] + \sum_{n=0}^{\infty} [\lambda^{\text{I}}(nd-z) - 1] - 2 \sum_{n=0}^{\infty} [\lambda^{\text{I}}(nd) - 1]. \quad (16)$$

This expression, derived for $\lambda_{\perp}^{\text{II}}$ only [9], will also be used to represent $\lambda_{\parallel}^{\text{II}}$ in this paper; the resulting expressions are referred to as the coherent superposition approximation (CSA). We note that in the derivation of Eq. (16) multiple interactions of the perturbations of the pressure and velocity fields induced by each wall are included, but multiple interactions of these perturbations with the colloid sphere are not included. That is, it is as if the perturbed fluid flow passes through the colloid particle freely. An approximation of this type, when applied to the calculation of the frequency dependent friction coefficient for a Brownian particle, is known to introduce some errors [26]. In particular, it is found that with this approximation the friction coefficient for the case of slip boundary conditions is overestimated ($5\pi\eta R$ instead of $4\pi\eta R$), and the frequency dependence of the friction coefficient for the case of stick boundary conditions is incorrect. Figure 4 displays the predicted values of D_{\parallel}/D_0 [using Eqs. (16) and (8)] and D_{\perp}/D_0 [using Eqs. (16) and (6)] for an isolated sphere confined to the midplane between two walls. Also shown in this figure are the approximations for D_{\parallel}/D_0 and D_{\perp}/D_0 , given by the LSA. As shown, when the separation of the two walls is comparable to the diameter of the

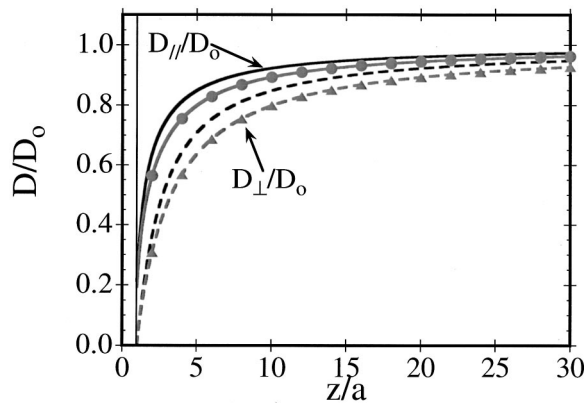


FIG. 4. Predicted values, using the CSA (see text), for D_{\parallel}/D_0 (solid line) and D_{\perp}/D_0 (dashed line) for an isolated sphere in the midplane ($z=d/2$) between two parallel flat walls. For comparison, D_{\parallel}/D_0 and D_{\perp}/D_0 , predicted using the LSA, are also shown (solid and dashed lines with symbols, respectively). The single wall correction factors given in Eqs. (6) and (8) are used for calculations presented in this figure.

sphere the LSA predicts a larger wall-drag force than does the CSA. The discrepancy has a peak value of about 15% near $z/a \sim 2$.

Overall, the parallel and perpendicular diffusion coefficients of a sphere between two flat walls behave like those of a sphere near one wall, in the sense that they decrease and become unequal as z/a approaches 1. As expected, for the same value of z/a the anisotropy of the diffusion coefficient is exaggerated when the particle is confined between two walls.

III. EXPERIMENTAL DETAILS

The system studied consisted of a dilute suspension of uncharged PMMA spheres (diameter $0.93 \mu\text{m}$, density 1.20 g/cm^3) confined in a thin glass cell, as depicted in Fig. 5; it is described elsewhere in detail [27]. To avoid aggregation of the uncharged PMMA spheres induced by van der Waals forces, the surface of each sphere was covered with an oligomeric brush ($\sim 300 \text{ \AA}$ thick) of poly(3-hydroxystearate) [28]. The glass cell was constructed from a microscope cover slip and a microscope slide, sealed together with UV sensitive glue and enclosing a very thin cavity (a couple to a few tens of μm). The cell was accessed through two pieces of glass tubing sealed to two holes drilled through the microscope slide. The walls of the cell were coated with trihydroxyoctadecylsilane (United Chemical Technologies, Inc., PA). To eliminate the influence of sedimentation on our measurements, the PMMA spheres were suspended in a 30% (by weight) sucrose solution (density 1.13 g/cm^3), so that the rate of sedimentation of a sphere is about $0.01 \mu\text{m/s}$. Since the sphere of interest is only free for $\frac{1}{2}$ -s intervals (see below), sedimentation is sensibly eliminated in our experiments.

Our measurements were carried out at temperatures between $20^\circ\text{C} \pm 0.7^\circ\text{C}$ and $23^\circ\text{C} \pm 0.7^\circ\text{C}$. When describing the results of our experiments, all of the relevant data are plotted in the same figure because they are presented in terms of inverse correction factors λ_{\parallel}^{-1} and λ_{\perp}^{-1} , which are inde-

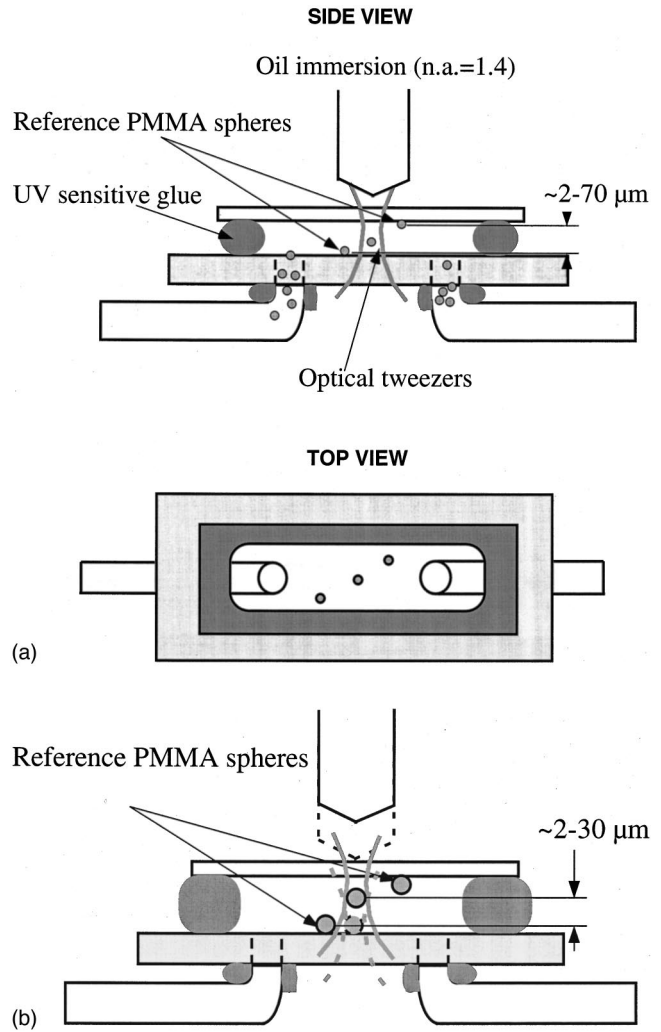


FIG. 5. Schematic diagram of an isolated PMMA sphere confined in a thin glass cell. The location of the sphere with respect to the walls is manipulated by optical tweezers. The spheres stuck to the walls are used as reference points to determine the cell spacing and the location of the moving sphere relative to the cell walls.

pendent of temperature (see Sec. II). Though each diffusion coefficient was measured at a slightly different temperature, the fluctuation of the temperature during any one measurement was less than $\pm 0.7^\circ\text{C}$. However, because it takes 20 min to measure one diffusion coefficient (see below), this fluctuation in temperature contributes an error of $\sim 4\%$ to the value of the diffusion coefficient.

We used digital video microscopy to measure the parallel and perpendicular diffusion coefficients of an isolated PMMA sphere near a wall. As illustrated in Fig. 6, our experimental apparatus consists of an Olympus BH2 microscope with an oil immersion objective ($100\times$, N.A. = 1.40), a Hitachi CCD video camera mounted on the microscope, a Sanyo GVR-S955 video cassette recorder, and a Macintosh computer with an LG-3 digital frame grabber. Real time movies of an isolated sphere moving in the cell were recorded via the CCD camera. The analog movies were digitized through the real-time frame grabber at a rate of 30 frames per second. Our image process routine, implemented using the IDL programming language, was developed by Crocker and Grier [29]. Time-dependent trajectories of the

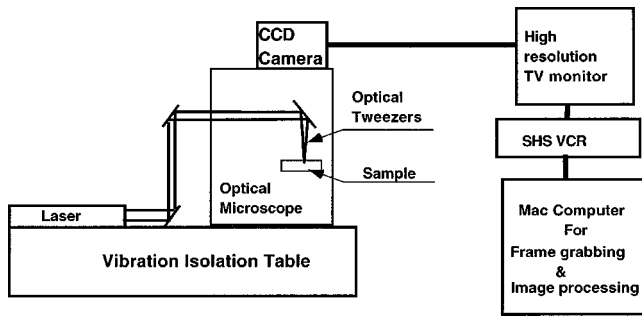


FIG. 6. Schematic diagram of the experimental apparatus.

sphere in three dimensions were extracted from a sequence of digitized images. The pixel size was calibrated by using a transmission electron microscope grid; the pixel is square, with a side length of $0.08 \mu\text{m}$. The imaging process methodology developed by Crocker and Grier permits the location of the sphere center with a precision of 0.2 pixel.

Two features that were implemented in our experiment allowed us to measure the diffusion coefficient as a function of distance from a wall directly. As already indicated, we utilized optical tweezers to control the location of the sphere relative to the walls, and to limit the displacement of the sphere with respect to the walls. Optical tweezers are formed when a laser beam is directed into the back aperture of a high numerical aperture objective lens, by which means it is brought to a tight focus at the focal plane of the microscope [30]. The focused beam generates an optical gradient force strong enough to trap a dielectric microsphere near the focus of the beam. Using the optical tweezers we can place the sphere at a specified position relative to the walls. To limit the displacement of the sphere along the vertical direction, the optical tweezers were turned on and off at a rate of 1 Hz. The sphere of interest was thereby captured for 0.5 s, set free for 0.5 s, and then recaptured, etc., for many cycles. Because the spheres were suspended in a viscous sucrose solution ($\eta/\eta_{\text{water}}=3.18$), a sphere moved less than $\pm 1 \mu\text{m}$ in each direction in the half a second it was free and, therefore, was easily recaptured. We found that it was necessary to use an objective with N.A.=1.4 to form an optical trap that is strong enough to capture and recapture a sphere in the middle of a cell thicker than $15 \mu\text{m}$.

The second feature implemented in our experiments is the direct measurement of both the separation of the confining walls and the location of the sphere with respect to the walls. The cell spacing was determined as follows. A very small fraction of the PMMA spheres stick to the coated cover slip and microscope slide, as illustrated in Fig. 5(a), thereby generating natural reference locations on the confining walls. Two PMMA spheres that were stuck to the top and bottom walls, respectively, and located within the field of view ($40 \times 50 \mu\text{m}^2$) were used as reference locations for the measurements (see Fig. 5). We determined the cell spacing by measuring the separation between the top and bottom reference spheres using the fine focus scale of the microscope. The readings of the separation were taken from the readout of a motorized high precision rotational stage ($\pm 0.02^\circ$) mounted on the focusing knob of the microscope. The repeatability of the measurements of the cell separation is about $\pm 0.2 \mu\text{m}$. With the help of the reference sphere locations, we deter-

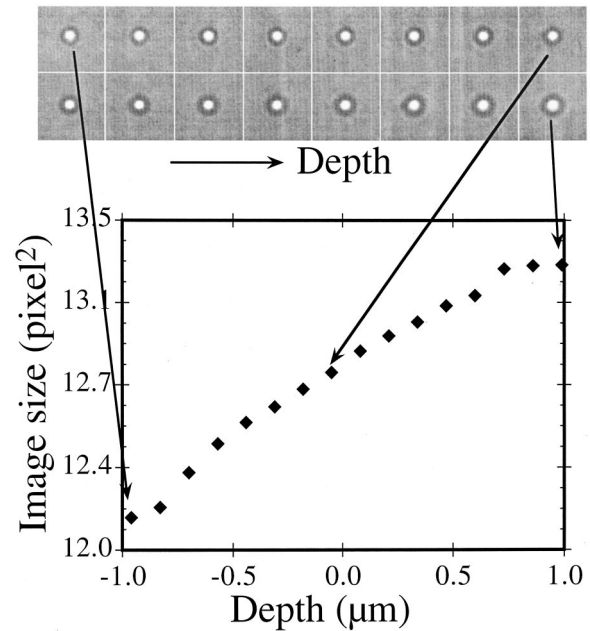


FIG. 7. Top: Images of the reference sphere as it is moved through the focal plane vertically. Bottom: The numerical conversion curve used to derive the vertical trajectory from the image size of the sphere (see text).

mined that the cell thickness was uniform across the entire field of view.

The distance between a sphere undergoing Brownian motion and the wall was determined by use of the optical tweezers. As illustrated in Fig. 5(b), a sphere grabbed by the optical tweezers was first brought to the bottom of the cell indicated by the reference sphere, and then moved to the selected distance from the wall.

We note that the colloids and the objective are in media with different refractive indices (the refractive index of the sucrose solution, $n_{\text{sol'n}}$, is 1.381, and the refractive index of the immersion oil used with the objective, n_{oil} , is 1.518). Consequently, the apparent difference between focal planes measured directly with the mechanical fine focus control has to be corrected (multiplied) by the ratio of refractive indices, $n_{\text{oil}}/n_{\text{sol'n}}=1.10$; that is, the readings both for the cell spacing and the sphere-wall separation have been multiplied by 1.10. In addition, because of the mismatch in refractive indices, the spherical aberration of the microscope objective is a function of the distance of the focal plane from the cell wall. As a result, the reference spheres stuck to the top and bottom of the cell do not ‘‘look’’ the same. Finally, the minimum of the trap formed by optical tweezers is sensitive to spherical aberration. As the spherical aberration increases, the trap will move downstream relative to the focal plane. We do not know how to characterize the systematic error due to spherical aberration near a wall. However, we believe that this error is no greater than the repeatability of our measurements ($\pm 0.2 \mu\text{m}$) because the distortion should not introduce an error greater than a fraction of the diameter of the sphere. In principle, the variation of spherical aberration with position can be eliminated if the refractive index of the suspension is matched to that of the immersion fluid and that of the cell wall.

The diffusion coefficients of the sphere for motion paral-

parallel and perpendicular to the confining walls (designated as the xy plane and xz plane, respectively) were calculated from the time-dependent trajectories $x(t)$, $y(t)$, and $z(t)$. These trajectories were directly extracted from the successive digitized images of the colloidal particles in the cell [29]. Since the area of the projection of a sphere onto the xy plane varies as it moves in and out of the focal plane, $z(t)$ can be obtained through the relation between the projected area and the distance of the sphere from the focal plane. We determined that relation as follows. A movie of the reference sphere stuck to the wall was recorded as the sphere was moved vertically through the focal plane (the images at different depths are shown in Fig. 7). The vertical motion of the reference sphere was affected by the motorized rotational

stage mounted on the focusing knob of the microscope. By synchronizing the movie with the motion of the rotational stage, we correlated the image size of the reference sphere with the vertical displacement of the sphere numerically. This numerical conversion was then used to convert the image size of the diffusing sphere into $z(t)$. Since the optical tweezers limit the vertical motion of the sphere to $\pm 1 \mu\text{m}$, the portion of the conversion curve actually used for translating image size to the distance of the diffusing sphere from the wall is approximately linear, as shown in Fig. 7. Conversion curves were constructed for each of the cells used. Each conversion curve was valid for the data that were taken with cells with gaps within a narrow range (a few μm).

To study the diffusion of a colloidal particle confined in

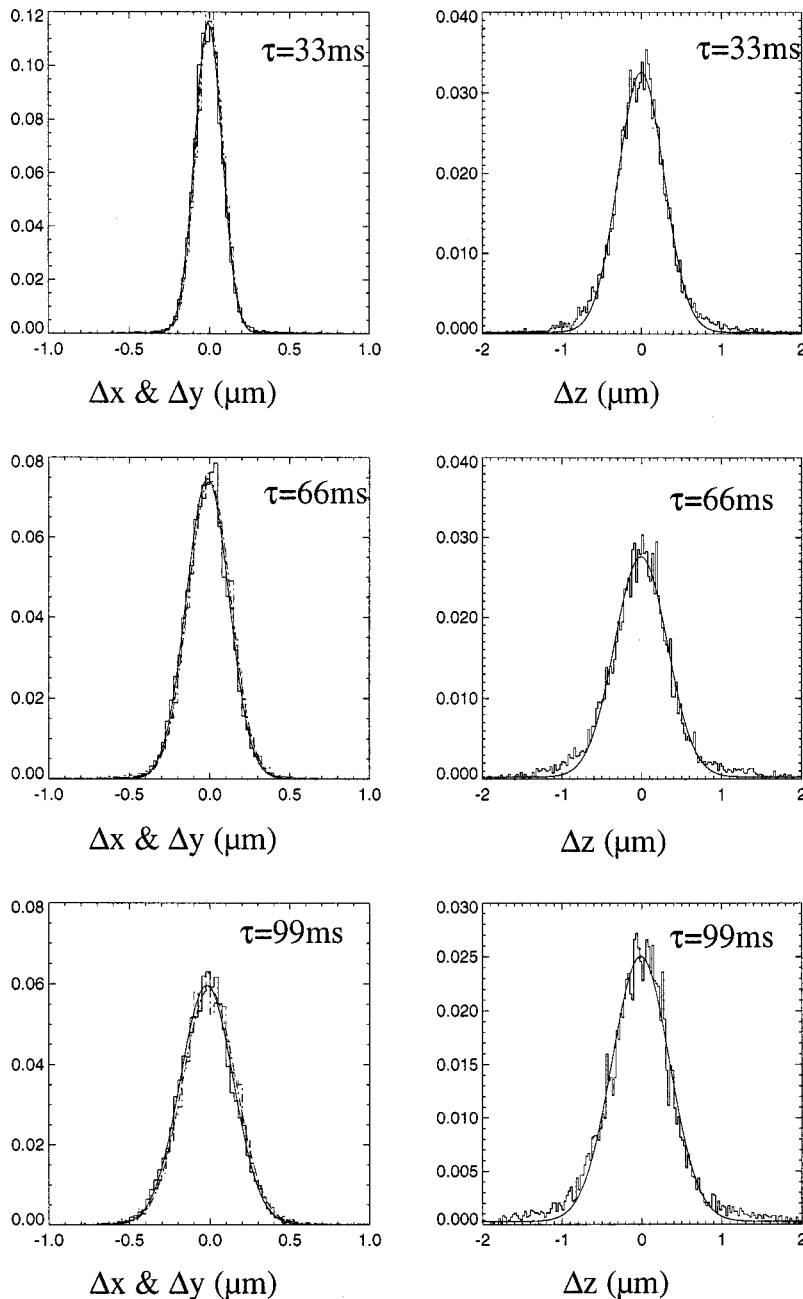


FIG. 8. Histograms of the displacements Δx , Δy , and Δz along the x , y , and z directions for five time steps (from 33 to 165 ms). The histograms for Δx (solid line) and Δy (dashed line) are plotted on the same graph (left); the histograms for Δz are on the right. The lines are the fits of the histograms to Eq. (18).

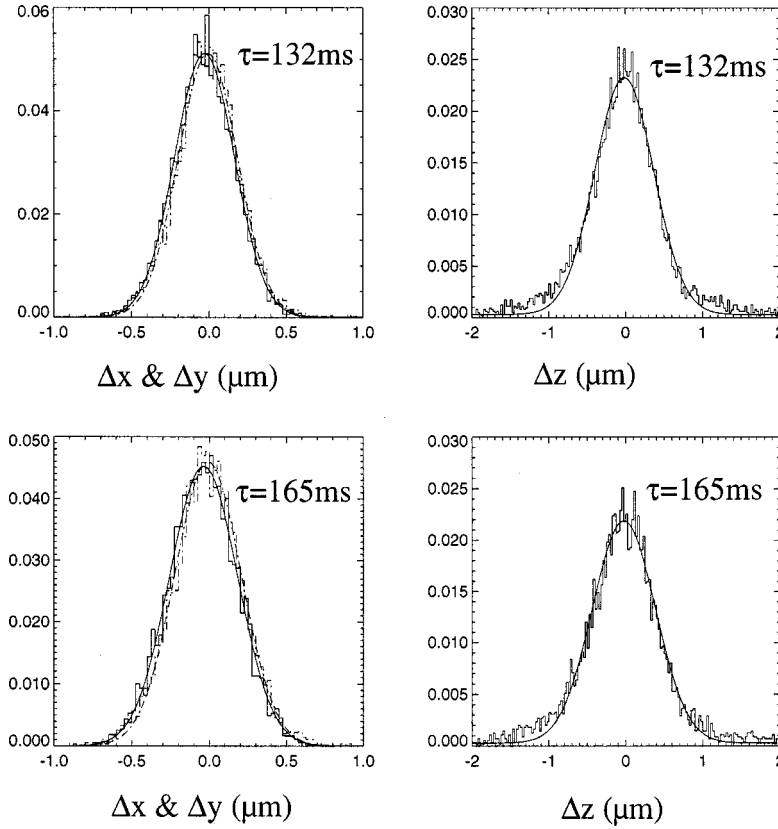


FIG. 8. (Continued).

the midplane between two flat walls, individual sample cells, each with a different spacing, were made by using various sizes of latex spheres as spacers. An alternative method was occasionally used to control the spacing between the two flat walls. The cell was attached to a vacuum manifold system consisting of Tygon tubing and a hand pump. By applying a slight vacuum through the hand pump, the spacing of the cell walls can be reduced threefold to fivefold. However, this method of adjusting the cell thickness sometimes introduces a slight but undesired flow of the fluid even though the system is airtight; therefore, it was not used for most of our measurements.

IV. RESULTS

The diffusion coefficients of an isolated sphere parallel to and perpendicular to the walls of a cell were measured over a wide range of distances between the sphere and the confining walls ($1 \mu\text{m} < z < 35 \mu\text{m}$). For each value of z , two movies (each 20 min long) of the sphere undergoing Brownian motion were recorded. By “isolated,” we mean that aside from the reference spheres fixed on the confining walls, there was only one sphere in an area of $30 \times 30 \mu\text{m}^2$. Because the optical tweezers were set to “blink” at 1 Hz, the Brownian motion of the sphere was free for only 0.5 s (consisting of 15 consecutive frames, separated by 33 ms between successive frames) before being recaptured. This free motion is long enough for a calculation of the diffusion coefficient, and excellent statistics are achieved by accumulating more than 2000 repetitions of such motions.

The diffusion coefficient in one dimension, e.g., in the x direction, D_x , is defined by [3]

$$\langle \Delta x^2(\tau) \rangle = 2D_x\tau, \quad (17)$$

and $\langle \Delta x^2(\tau) \rangle$, the mean-squared displacement, is obtained from the probability distribution function

$$P(\Delta x(\tau)) = \frac{1}{\sqrt{2\pi\langle \Delta x^2(\tau) \rangle}} \exp\left\{-\frac{|\Delta x(\tau) - \chi|^2}{2\langle \Delta x^2(\tau) \rangle}\right\}. \quad (18)$$

The offset χ in Eq. (18) is included to account for any drift of the sphere in the x direction due to flow of the fluid in the experimental cell. In our measurements χ was insignificant ($< 0.05 \mu\text{m}$ during 0.5 s).

The value of D_x was obtained as follows. First, histograms of $\Delta x(\tau)$ corresponding to different time steps τ were fitted to Eq. (18), and $\langle \Delta x^2(\tau) \rangle$ was derived through the fitting. Then D_x was determined from the linear fit of $\langle \Delta x^2(\tau) \rangle$ to τ [Eq. (17)]. The same method was used to derive the diffusion coefficients along the y and z directions.

Histograms of $\Delta x(\tau)$, $\Delta y(\tau)$, and $\Delta z(\tau)$ for five time steps (from 33 to 165 ms), extracted from the trajectories, $x(t)$, $y(t)$, and $z(t)$, are shown in Fig. 8. The lines are fits of the data to Eq. (18) and all the histograms are fit well with the Gaussian probability distribution function. Figures 9(a) and 9(b) show $\langle \Delta x^2(\tau) \rangle$, $\langle \Delta y^2(\tau) \rangle$, and $\langle \Delta z^2(\tau) \rangle$ as functions of τ , separately. Note that the data in Fig. 9(b) are shifted vertically to eliminate an apparent nonzero intercept at $\tau=0$, which is due to the error in vertical tracking. The lines are fits of the data to Eq. (17). To eliminate any pinning effect due to the “blinking” optical tweezers, only nine consecutive frames (out of 15) during the tweezers off period

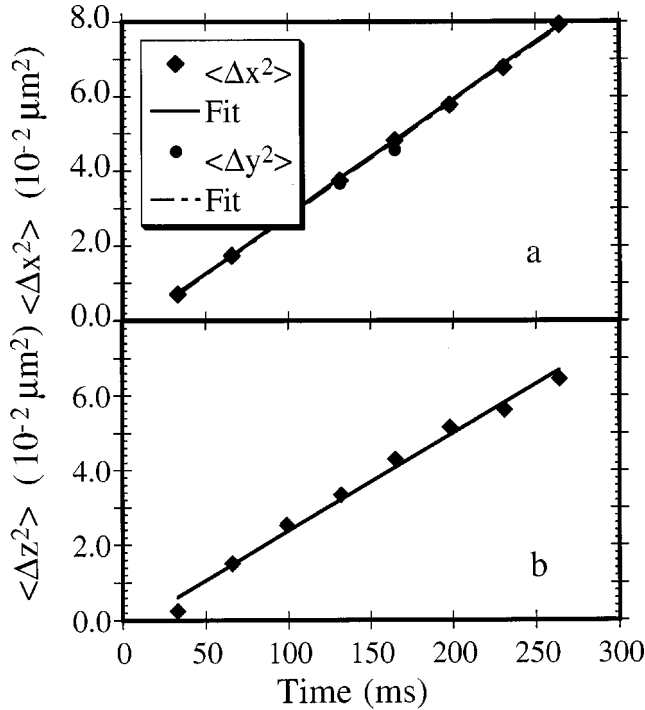


FIG. 9. Mean-squared displacements $\langle \Delta x^2(\tau) \rangle$ and $\langle \Delta y^2(\tau) \rangle$ [in (a)] and $\langle \Delta z^2(\tau) \rangle$ [in (b)] as a function of τ . Note that the data in (b) are shifted vertically to eliminate an apparent nonzero intercept at $\tau=0$. The lines are fits of the data to a linear function of τ [Eq. (17)].

were used. Figure 9 indicates that the motion parallel to the confining walls (the x - y plane) is isotropic within our experimental precision (D_x and D_y agree within 4%).

The calculated effective wall-drag forces are explicit functions of the separation of an isolated sphere from the wall and/or walls. In our experiments, because of the Brown-

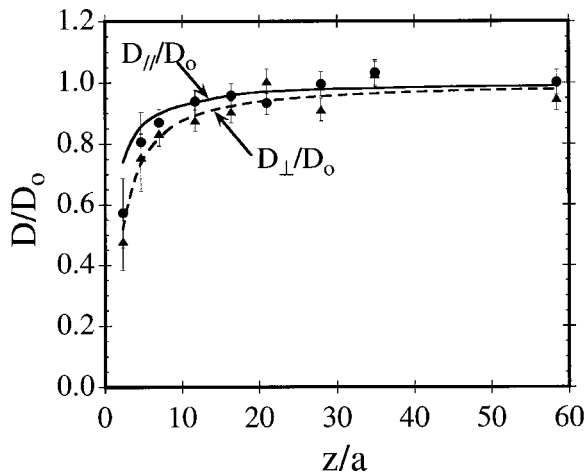
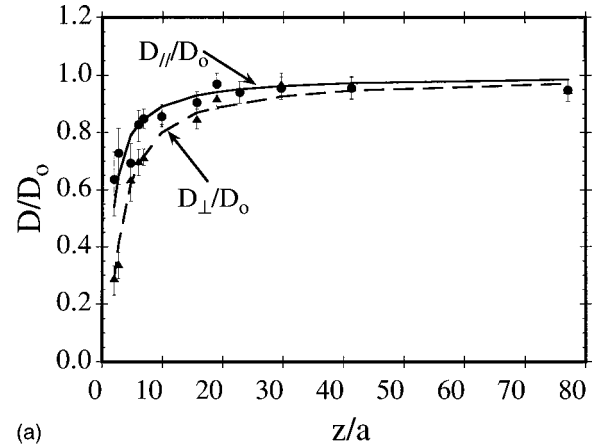
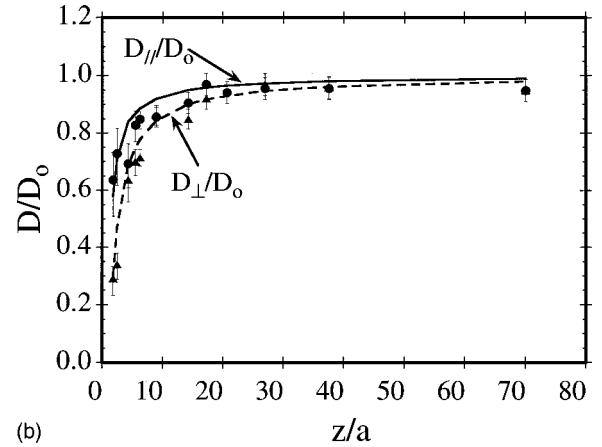


FIG. 10. The measured diffusion coefficients D_{\parallel} (solid circles) and D_{\perp} (solid triangles) for an isolated sphere near one flat wall, normalized by D_0 . The solid line is the theoretical prediction for \bar{D}_{\parallel}/D_0 calculated (not fitted) using Eq. (8), averaged using Eq. (20a). The dashed line is the theoretical prediction for \bar{D}_{\perp}/D_0 calculated (not fitted) using Eq. (6), averaged using Eq. (20b). The approximate width of the distribution function used in Eq. (20) is $0.25 \mu\text{m}$.



(a)



(b)

FIG. 11. (a) The measured diffusion coefficients D_{\parallel} (solid circles) and D_{\perp} (solid triangles) normalized by D_0 , for an isolated sphere confined in the midplane between two parallel flat walls, compared with theoretical values calculated, not fitted, using the LSA. The solid line is for \bar{D}_{\parallel}/D_0 given by Eqs. (8) and (13), averaged using Eq. (20a). The dashed line is for \bar{D}_{\perp}/D_0 given by Eqs. (6) and (13), averaged using Eq. (20b). The approximate width of the distribution function used in Eq. (20) is $0.20 \mu\text{m}$. (b) The measured diffusion coefficients D_{\parallel} (solid circles) and D_{\perp} (solid triangles), normalized by D_0 , for an isolated sphere confined in the midplane between two parallel flat walls, compared with theoretical values calculated, not fitted, using the CSA. The solid line is for \bar{D}_{\parallel}/D_0 given by Eqs. (8) and (16), averaged using Eq. (20a). The dashed line is for \bar{D}_{\perp}/D_0 given by Eqs. (6) and (16), averaged using Eq. (20b). The width of the distribution function used in Eq. (20) is $0.20 \mu\text{m}$.

ian motion of the sphere, the distance of the sphere from the wall(s) varies with time as the measurements were made. As a result, a diffusion coefficient measured is an average weighed by the distribution function for sphere-wall separations. To compare the predicted and measured values of the diffusion coefficient, we compute

$$\bar{D}_{\parallel} = \int_a^{d-a} P(z) D_{\parallel}(z) dz = D_0 \int_a^{d-a} P(z) \lambda_{\parallel}^{-1}(z) dz \quad (19a)$$

and

TABLE I. D_{\parallel}/D_0 for a sphere near a single flat plane.

z/a	D_{\parallel}/D_0 (theory)	\bar{D}_{\parallel}/D_0 (theory)	D_{\parallel}/D_0 (data)
2.3	0.77	0.74	0.57
4.7	0.88	0.87	0.81
7.0	0.92	0.91	0.87
12	0.95	0.93	0.94
16	0.97	0.96	0.93
21	0.97	0.97	0.93
28	0.98	0.98	1.0
35	0.98	0.98	1.0
58	0.99	0.99	1.0

$$\bar{D}_{\perp} = \int_a^{d-a} P(z) D_{\perp}(z) dz = D_0 \int_a^{d-a} P(z) \lambda_{\perp}^{-1}(z) dz, \quad (19b)$$

where d is the spacing of the cell, and $P(z)$ is the distribution function for sphere-wall separations [14,19]. Because the density difference between the PMMA sphere and the host fluid is very small (0.07 g/cm³), we can neglect sedimentation effects and use Eq. (18) for Δz ; we find

$$\begin{aligned} \frac{\bar{D}_{\parallel}(z)}{D_0} &= \int_a^{d-a} P(z'-z) \lambda_{\parallel}^{-1}(z') dz' \\ &= \frac{1}{\sqrt{2\pi}\sigma} \int_a^{d-a} \lambda_{\parallel}^{-1}(z') \exp\left\{-\frac{|z'-z|^2}{2\sigma^2}\right\} dz' \end{aligned} \quad (20a)$$

and

$$\begin{aligned} \frac{\bar{D}_{\perp}(z)}{D_0} &= \int_a^{d-a} P(z'-z) \lambda_{\perp}^{-1}(z') dz' \\ &= \frac{1}{\sqrt{2\pi}\sigma} \int_a^{d-a} \lambda_{\perp}^{-1}(z') \exp\left\{-\frac{|z'-z|^2}{2\sigma^2}\right\} dz'. \end{aligned} \quad (20b)$$

The data displayed in Fig. 8 imply that $\sigma \sim 0.25 \mu\text{m}$ for single-wall measurements and $\sigma \sim 0.2 \mu\text{m}$ for double-wall measurements, respectively. \bar{D} is significantly different from

TABLE II. D_{\perp}/D_0 for a sphere near a single flat plane.

z/a	D_{\perp}/D_0 (theory)	\bar{D}_{\perp}/D_0 (theory)	D_{\perp}/D_0 (data)
2.3	0.55	0.52	0.48
4.7	0.77	0.76	0.76
7.0	0.84	0.84	0.84
12	0.90	0.90	0.88
16	0.93	0.93	0.91
21	0.95	0.94	1.0
28	0.96	0.96	0.91
35	0.97	0.97	1.0
58	0.98	0.98	0.95

TABLE III. D_{\parallel}/D_0 for a sphere confined in the midplane between two flat walls.

z/a	D_{\parallel}/D_0 LSA	\bar{D}_{\parallel}/D_0 LSA	D_{\parallel}/D_0 CSA	\bar{D}_{\parallel}/D_0 CSA	D_{\parallel}/D_0 data
2.0	0.57	0.54	0.64	0.59	0.64
2.7	0.66	0.65	0.73	0.72	0.73
4.7	0.79	0.79	0.84	0.84	0.69
6.0	0.83	0.83	0.87	0.87	0.83
6.9	0.85	0.85	0.89	0.89	0.85
9.8	0.89	0.89	0.92	0.92	0.86
16	0.93	0.93	0.95	0.95	0.91
19	0.94	0.94	0.96	0.96	0.97
23	0.95	0.95	0.97	0.97	0.94
30	0.96	0.96	0.97	0.97	0.96
41	0.97	0.97	0.98	0.98	0.96
77	0.99	0.99	0.99	0.99	0.95

D when z/a approaches 1, but when $z/a \geq 4$ the difference between \bar{D} and D drops to less than 1%.

The most important limitation to our experimental precision when $z/a > 4$ arises from the fluctuation in temperature ($\pm 0.7^\circ$), which generates a 4% uncertainty in the diffusion coefficient. When $z/a < 4$, the uncertainty in the diffusion coefficient increases to $\sim 10\text{--}20\%$. This increase in experimental uncertainty arises because the error due to the repeatability of the measurements of the separation (the separation the center of the sphere from the wall, $\Delta z \cong \pm 0.2 \mu\text{m}$, and the wall-separation $\Delta d \cong \pm 0.2 \mu\text{m}$) is larger (relatively) when $z/a < 4$. The measured diffusion coefficients, with their associated error estimates, are displayed in Figs. 10 and 11.

We first examine the results for the diffusion of a sphere near one wall. Cells with a spacing d from about 10 to 65 μm were used. In this range of $d/2a$ ($\sim 10\text{--}66$) the predicted values for the diffusion coefficient of a sphere interacting with two walls differ by less than 4% from that for $d/2a = \infty$, which is less than our experimental precision. For this reason, the data from all these cells were combined together, and were considered to be that for a sphere confined near one wall. Figure 10 shows the measured values of D_{\parallel}/D_0 and D_{\perp}/D_0 as a function of z/a for an isolated sphere confined

TABLE IV. D_{\perp}/D_0 for a sphere confined in the midplane between two flat walls.

z/a	D_{\perp}/D_0 LSA	\bar{D}_{\perp}/D_0 LSA	D_{\perp}/D_0 CSA	\bar{D}_{\perp}/D_0 CSA	D_{\perp}/D_0 data
2.0	0.31	0.28	0.37	0.34	0.29
2.7	0.43	0.41	0.50	0.47	0.34
4.7	0.62	0.62	0.69	0.69	0.64
6.0	0.69	0.69	0.76	0.76	0.70
6.9	0.72	0.72	0.78	0.78	0.71
9.8	0.80	0.80	0.85	0.85	0.86
16	0.87	0.87	0.90	0.90	0.85
19	0.89	0.89	0.92	0.92	0.92
30	0.93	0.93	0.95	0.95	0.97
41	0.95	0.95	0.96	0.96	0.96
77	0.97	0.97	0.98	0.98	0.95

near a single wall, compared with the values calculated from Eqs. (8) and (6), respectively, for the range $\sim 2.1 < z/a < 54$. The in-plane diffusion coefficient D_{\parallel} is the average of D_x and D_y . As shown in Tables I and II, for a sphere $1 \mu\text{m}$ away from the wall ($z/a \sim 2.1$) the measured values of D_{\parallel} and D_{\perp} drop to $\sim 0.57D_0$ and $0.48D_0$, respectively. When a sphere is about $9 \mu\text{m}$ away from the wall ($z/a \sim 19$) it behaves like a free Brownian particle within our experimental precision. Our data agree with the theoretical predictions within the experimental precision.

We now examine the results for the diffusion of a sphere confined in the midplane between two walls ($z \cong d/2$). Figure 11 shows the measured values of D_{\parallel}/D_0 and D_{\perp}/D_0 for the range $\sim 2.0 < z/a < 78$, and Tables III and IV list the experimental and theoretical values for D_{\parallel}/D_0 and D_{\perp}/D_0 . When $z/a \sim 2.0$, the measured values of D_{\parallel} and D_{\perp} drop to $\sim 0.64D_0$ and $0.29D_0$, respectively. When $z/a > 20$, a sphere behaves like a free Brownian particle within our experimental precision. A comparison of the measured and predicted diffusion coefficients using the LSA [with Eqs. (6) and (8) as single wall correction factors] is shown in Fig. 11(a), and a similar comparison using the CSA [also with Eqs. (6) and (8) as single wall correction factors] is shown in Fig. 11(b). We note that the values of D_{\parallel} calculated using the linear superposition approximation are very close to those given by Faxen's analytical solution [see Eq. (11) and Fig. 3].

In the range $4.7 \leq z/a \leq 16$, our data appear to agree much better with the values calculated using the LSA than those calculated using the CSA. For $z/a \leq 2.7$, the uncertainty in the measured values of the diffusion coefficients prevents us from discriminating between the different theoretical predictions. For $z/a \geq 19$ the differences between the values of the

diffusion coefficients predicted using the LSA and the CSA are less than our experimental precision.

V. SUMMARY

We have demonstrated that digital video microscopy, in combination with optical tweezers, provides us with a method to directly determine, for an isolated Brownian particle confined between two flat walls, the diffusion coefficients parallel and perpendicular to the walls. The method is based on tracking, and then analyzing, the time-dependent trajectory of the sphere. Our results yield these diffusion coefficients as an explicit function of the separation of the sphere from a wall. Overall, for the case of a sphere confined between two flat walls, our results are in quantitative agreement, within the experimental precision, with the behavior predicted using a hydrodynamic analysis that independently superposes the wall drag effects arising from each wall. Our results imply, indirectly, that neglect of multiple interactions of the perturbations of the pressure and velocity fields induced by each wall with the colloid sphere leads to an underestimate of the influence of the wall on the drag force experienced by the particle.

ACKNOWLEDGMENTS

We thank Professor David Grier, Professor John Crocker, Dr. Eric Dufresne, and Juanita Mora for their generous help in setting up the video microscope system. We also thank Professor Mark Schlossman and Dr. James Viccaro for many helpful discussions. This work was supported by a grant from the NSF POWRE program (No. DMR-9870437). We have also benefited from support provided by the NSF Materials Research Science and Engineering Center at The University of Chicago (MRSEC-543038).

-
- [1] P. Ganatos, S. Weinbaum, and R. Pfeffer, *J. Fluid Mech.* **99**, 739 (1980).
 - [2] A. Pralle, E.-L. Florin, E. H. K. Stelzer, and J. K. H. Horber, *Appl. Phys. A: Mater. Sci. Process.* **66**, S71 (1998).
 - [3] W. B. Russel, D. A. Saville, and W. R. Schowalter, *Colloidal Dispersions* (Cambridge University Press, Cambridge, 1989).
 - [4] J. Happel and H. Brenner, *Low Reynolds Number Hydrodynamics* (Kluwer, Dordrecht, 1983).
 - [5] H. Brenner, *Chem. Eng. Sci.* **16**, 242 (1961).
 - [6] P. Ganatos, R. Pfeffer, and S. Weinbaum, *J. Fluid Mech.* **99**, 755 (1980).
 - [7] A. J. Goldman, R. G. Cox, and H. Brenner, *Chem. Eng. Sci.* **22**, 637 (1967).
 - [8] B. P. Ho and L. G. Leal, *J. Fluid Mech.* **65**, 365 (1974).
 - [9] L. Lobry and N. Ostrowsky, *Phys. Rev. B* **53**, 12 050 (1996).
 - [10] G. D. M. MacKay and S. G. Mason, *J. Colloid Interface Sci.* **16**, 632 (1961).
 - [11] G. D. M. MacKay, M. Suzuki, and S. G. Mason, *J. Colloid Interface Sci.* **18**, 103 (1963).
 - [12] Z. Adamczyk, M. Adamczyk, and T. G. M. v. d. Van, *J. Colloid Interface Sci.* **96**, 204 (1983).
 - [13] K. H. Lan, N. Ostrowsky, and D. Sornette, *Phys. Rev. Lett.* **57**, 17 (1986).
 - [14] M. I. M. Feitosa and O. N. Mesquita, *Phys. Rev. A* **44**, 6677 (1991).
 - [15] M. Hosoda and K. T. K. Sakai, *Phys. Rev. E* **58**, 6275 (1998).
 - [16] P. G. Cummins and E. J. Staples, *J. Phys. E* **14**, 1171 (1981).
 - [17] D. C. Prieve and N. A. Frej, *Langmuir* **6**, 396 (1990).
 - [18] N. A. Frej and D. C. Prieve, *J. Chem. Phys.* **98**, 7552 (1993).
 - [19] L. P. Faucheux and A. J. Libchaber, *Phys. Rev. E* **49**, 5158 (1994).
 - [20] J. Radler and E. Sackman, *Langmuir* **8**, 848 (1992).
 - [21] R. Rajagopalan, *Colloids Surf.* (to be published).
 - [22] E. Allahyarov, I. D'Amico, and H. Löwenl, *Phys. Rev. E* **60**, 3199 (1999).
 - [23] D. G. Grier, *Nature (London)* **393**, 621 (1998).
 - [24] J. C. Crocker and D. G. Grier, *Phys. Rev. Lett.* **77**, 1897 (1996).
 - [25] J. S. Halow and G. B. Wills, *AIChE J.* **16**, 281 (1970).
 - [26] A. J. Masters and P. A. Madden, *J. Chem. Phys.* **74**, 2450 (1981).
 - [27] A. H. Marcus, B. Lin, and S. A. Rice, *Phys. Rev. E* **53**, 1765 (1996).
 - [28] L. Antl, R. D. H. J. W. Goodwin, R. H. Ottewill, S. M. Owens, and J. A. W. Papworth, *Colloids Surface* **17**, 67 (1986).
 - [29] J. C. Crocker and D. G. Grier, *J. Colloid Interface Sci.* **179**, 198 (1996).
 - [30] D. G. Grier, *Curr. Opin. Colloid Interface Sci.* **2**, 264 (1997).